catalysts

MDPI

Article

Comparison of the Mechanisms of deNOx and deN$_2$O Processes on Bimetallic Cu–Zn and Monometallic Cu–Cu Dimers in Clinoptilolite Zeolite—A DFT Study Simulating Industrial Conditions

Izabela Kurzydym, Weronika Magnuszewska and Izabela Czekaj *

Faculty of Chemical Engineering and Technology, Cracow University of Technology, Warszawska 24, 31-155 Kraków, Poland; izabela.kurzydym@doktorant.pk.edu.pl (I.K.); w.magnuszewska@student.pk.edu.pl (W.M.)
* Correspondence: izabela.czekaj@pk.edu.pl

Abstract: This paper presents two mechanisms for the deNOx process and for the deN$_2$O process (in two variants). The processes were carried out on a clinoptilolite zeolite catalyst with a deposited Cu–Cu monometallic dimer and Cu–Zn bimetallic dimer with bridged oxygen between the metal atoms. Analyses were performed for hydrated forms of the catalyst with a hydrated bridging oxygen on one of the metal atoms. Calculations were performed using DFT (density functional theory) based on an ab initio method. The analyses included calculations of the energies of individual reaction steps and analysis of charges, bond orders and bond lengths as well as HOMO, SOMO and LUMO orbitals of selected steps in the mechanism. Based on the results obtained, it was determined that the most efficient catalyst for both processes is a Cu–Zn bimetallic catalyst with a bridged hydroxyl group. It shows higher efficiency in the limiting step (formation of the -N$_2$H intermediate product) than the previously studied FAU and MFI zeolites with a Cu–Zn bimetallic dimer. In addition, the possibility of using the catalytic system from the deNOx process in the deN$_2$O process was presented, which can benefit SCR installations. In addition, it was proved that the order of adsorption of NO and N$_2$O has significance for further steps of the deN$_2$O process. In order to improve the comparison of FAU, MFI and CLI zeolite catalysts with a Cu–Zn dimer, further studies on the deN$_2$O mechanism for the first two zeolites are needed. This study allows us to propose a bimetallic catalyst for the deNOx and deN$_2$O processes.

Keywords: deNOx; bimetallic; deN$_2$O; DFT; clinoptilolite

Citation: Kurzydym, I.; Magnuszewska, W.; Czekaj, I. Comparison of the Mechanisms of deNOx and deN$_2$O Processes on Bimetallic Cu–Zn and Monometallic Cu–Cu Dimers in Clinoptilolite Zeolite—A DFT Study Simulating Industrial Conditions. *Catalysts* **2023**, *13*, 1210. https://doi.org/10.3390/catal13081210

Academic Editor: C. Heath Turner

Received: 25 June 2023
Revised: 7 August 2023
Accepted: 9 August 2023
Published: 14 August 2023

1. Introduction

Anthropogenically produced nitrogen oxides (NOx), which are components of fuel exhausts as well as waste gases from the chemical industry, are the source of many air pollutants such as acid rain and photochemical smog [1–5]. These pollutants are very harmful to both the environment and human health. N$_2$O is also an essential toxic gas [6–8]. This oxide is produced during the production of nitric acid and, among other things, as a by-product of the NH$_3$-SCR process. This gas is one of the greenhouse gases that contributes to global warming, as well as damages the ozone layer. In addition, it has a global warming potential (GWP) approximately 310 times higher than that of the much more famous CO$_2$ [9].

One of the leading and most effective NOx reduction technologies is selective catalytic reduction (SCR) using ammonia as a reducing agent [10–13]. In addition to experimental studies, theoretical studies that provide a detailed look at the reaction mechanism [14–16] and studies that combine experiment and theory to fully understand the deNOx process are also very popular [17]. Theoretical calculations allow the investigation of many atoms and systems in a relatively short time and with low financial effort, which can then contribute to identifying the most efficient structure for experimental studies [18].

Industrial vanadium catalysts of the SCR process can come in the form of honeycomb-shaped monoliths or plates [19]. These catalysts show relatively high efficiency; however, the temperature window of operation is quite narrow and is in the range of 300–400 °C. Additionally, this catalyst tends to oxidise sulphur oxides (SO_2 and SO_3), which react with NH_3 to form ammonium sulphates that deactivate the catalyst [20].

In order to avoid the above-mentioned problems, low-temperature catalysts, operating already at a temperature of about 100 °C, are still being studied, which could avoid the formation of toxic SO_2 and fly ash and also reduce the costs of the SCR process [21]. Zeolite catalysts doped with iron [22,23], copper [17,24,25] or zinc [26], as well as bimetallic systems [15,27,28], have become a focus of interest and are potential catalysts for SCR reactions.

The above-mentioned transition metals deposited on zeolites have attracted much scientific discussion due to their high deNOx activity, wide temperature window, high thermostability and chemical durability (lower probability of sulphur oxide oxidation) [29–32]. The application of zeolites with deposited transition metals has been presented in various review publications, e.g., Branderberger et al. [33] described comprehensively the chemistry of the NH_3-SCR process together with some aspects of the mechanism of formation of transition products. Chen et al. [34] collected and detailed the characterisation of the active sites of zeolite catalysts with Cu and Fe metals and also described the use of DFT calculations for surface descriptions.

The activity of the deNOx process at low temperatures [35,36] has improved significantly over the past few years. This is mainly due to the development of copper catalysts supported on porous materials such as zeolites. One of them—Cu-SSZ13—has been commercialised as an SCR catalyst in diesel engines [37]. Copper-based catalysts are also very promising due to their high activity and thermal stability [38,39]. The temperature window is reduced to below 400 °C [40,41]; however, the determination of the species of copper deposited on the support is still a significant problem. Research by Xu et al. [27] showed that Zn doping of Cu-containing catalysts exhibits good catalytic activity, increases hydrothermal stability and also assists in the dispersion of Cu^{2+} species, which are important in the catalytic process. Zn forms bimetallic (Cu–O–Zn) complexes with Cu which have greater stability than single copper ions [15,27,42]. Catalysts containing copper or zinc were also considered in studies on N_2O decomposition [43–47].

The global warming potential of the N_2O molecule, mentioned earlier, requires a catalyst to be found to efficiently decompose this unwanted atmospheric compound to non-toxic nitrogen and water molecules [48]. In the context of combining the deNOx and deN_2O processes in N_2O decomposition studies, it is important to investigate the interactions of N_2O with NO or NO_2. This is important for describing the mechanism of these processes and for clarifying the ways in which the N–O bond is broken or the N–N bond is formed [49]. Studies performed so far have concluded that, for deNOx, transition metals on supports can be beneficial in N_2O decomposition [50–52]. Due to the fact that N_2O can be formed in the deNOx process, catalysts that are effective in the two deNOx and deN_2O processes are sought [23,53–56]. It is important to study the competitiveness of NO and N_2O [57]. At present, in plants producing, e.g., nitric acid, the removal of NO and N_2O proceeds separately. In order to reduce costs, and save space and time, an important problem is finding a catalyst that allows the simultaneous removal of these oxides. To completely explain the details of the SCR processes of both deNOx and deN_2O, it is necessary to have a detailed understanding of the reaction mechanism in these processes [11,58,59], especially the step of the formation of the N_2H intermediate, which is described as limiting, e.g., for vanadium catalysts [60]. Theoretical studies have proved that one of the most effective metallic systems in zeolites for NOx reduction is the bridged oxygen metallic dimer (M_1–O_b–M_2) [61,62]. To analyse the systems, the visualisation and energies of the HOMO, SOMO and LUMO orbitals are also used to determine the reactivity of the system [63].

In the present paper, the deNOx and deN_2O processes are analysed over clinoptilolite zeolite with two metal dimer systems, Cu–Cu and Cu–Zn. Hydrated structures with an OH group on bridged oxygen or on one of the metal atoms are designed in order to illustrate the reactions in the presence of water. The energies between the different process steps are calculated. Two deN_2O process pathways are proposed, in which the order of adsorbates is of fundamental value. For a detailed interpretation of the mechanisms and analyses of charges on atoms, bond orders and bond lengths, as well as the visualisation and energies of the HOMO, SOMO and LUMO orbitals, the most relevant steps of the mechanisms are presented. All calculations are carried out using the DFT-based ab initio method. The results are visualised using Mercury 4.0 [64] and Molekel [65] software (http://ugovaretto.github.io/molekel/ accessed on 8 August 2023).

2. Results

2.1. Adsorption of Dimers

For the calculation of the reactions in the deNOx and deN_2O processes, structures based on clinoptilolite zeolites were used (Figure 1). Metallic dimers, including monometallic Cu–O–Cu and bimetallic Cu–O–Zn with oxygen bridging between the metals were placed on the active catalytic sites in the region of the Al atoms. In addition, partial hydration of these structures by adsorption of an OH group on one of the metals in the dimer or by the formation of a bridging OH group was considered.

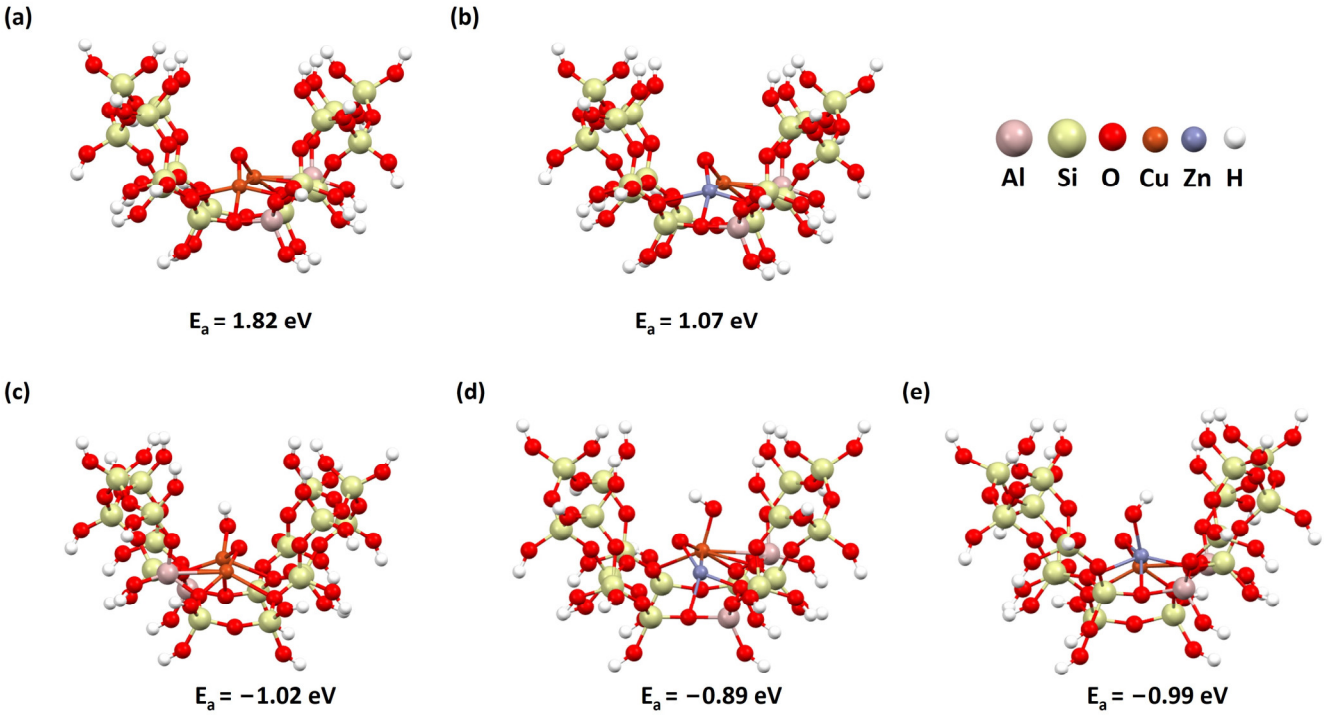

Figure 1. Cluster model of the clinoptilolite zeolite structure with deposited mono- or bimetallic dimer: (**a**) Cu–O–Cu dimer, (**b**) Cu–O–Zn dimer, (**c**) Cu–O–Cu dimer with an OH group on Cu, (**d**) Cu–O–Zn with an OH group on Cu and (**e**) Cu–O–Zn with an OH group on Zn. Adsorption energy is shown below the structure. The colour of the atoms: orange—copper, grey-blue—zinc, pink—aluminium, yellow—silica, red—oxygen, white—hydrogen.

Figure 1 shows the adsorption energies. The adsorption of the dimers in the clinoptilolite structure is an endothermic process (Figure 1a,b), while the following step involving the attachment of the hydroxyl group proceeds with the release of energy (Figure 1c–e).

2.2. DeNOx Mechanism

Figure 2 presents a block diagram of the deNOx process as performed in this work. Figure 2a shows a schematic description of the deNOx mechanism on a catalytic system containing a zeolite, metal dimer and an OH group on bridged oxygen. Figure 2b represents the deNOx mechanism on a catalytic system in which the OH group is located on one of the metals in the dimer.

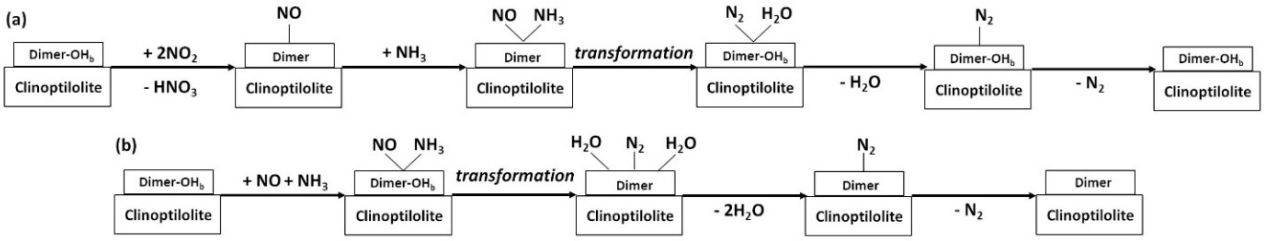

Figure 2. Schematic presentation of the deNOx process on a clinoptilolite catalyst with a metal dimer: (**a**) dimer with an OH group on bridged oxygen, (**b**) dimer with an OH group on one of the metal atoms.

The investigated structures were further used to represent the individual stages of the deNOx and deN$_2$O processes. Based on the literature [11,15,17], where a detailed mechanism was successfully used, a mechanism was proposed for the designed clinoptilolite zeolite structures.

The lengths and orders of the bonds, as well as the ionicity of the systems selected for further analysis, can be seen in the Supplementary Information in Figures S1 and S2.

In Figures 3 and 4, the mechanism of the deNOx process for the Cu–O–Cu (Figure 3) and Cu–O–Zn (Figure 4) systems with a bridged hydroxyl group is presented.

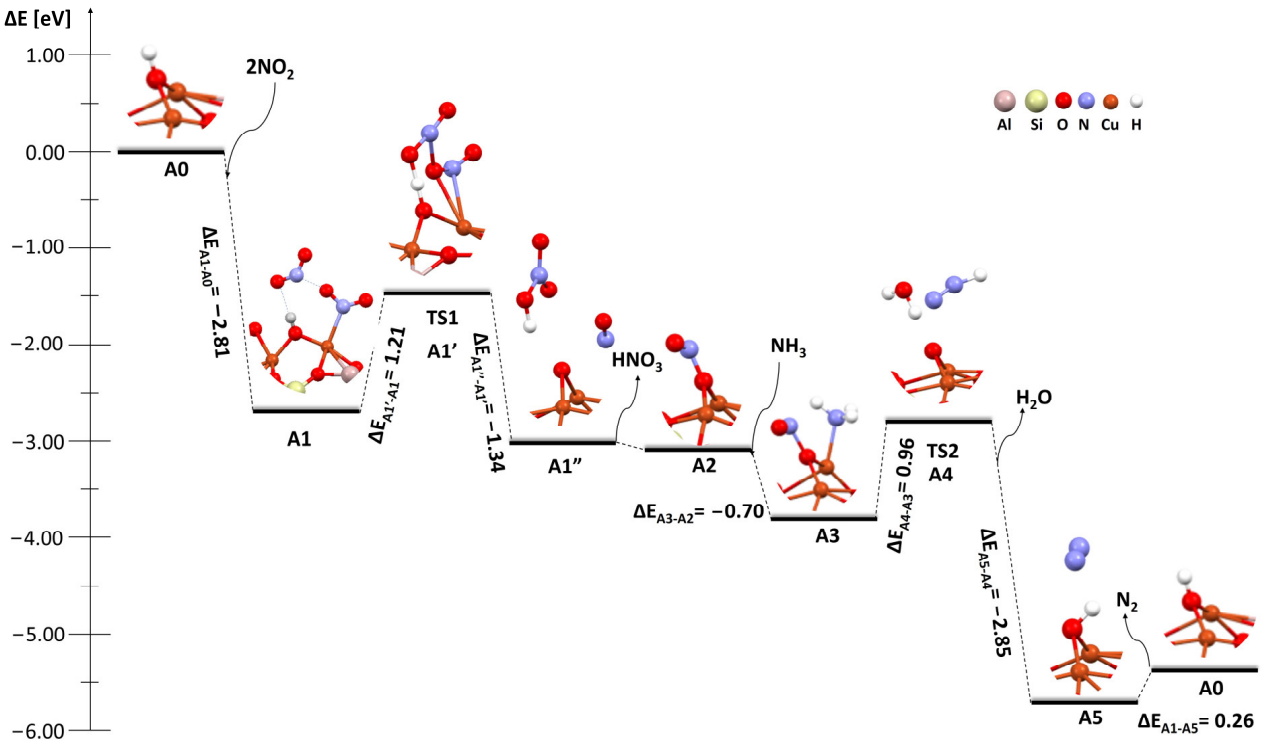

Figure 3. Energy diagram of the proposed mechanism of deNOx on the clinoptilolite zeolite with a bridged OH group in the dimer—Cu–O–Cu monometallic dimer.

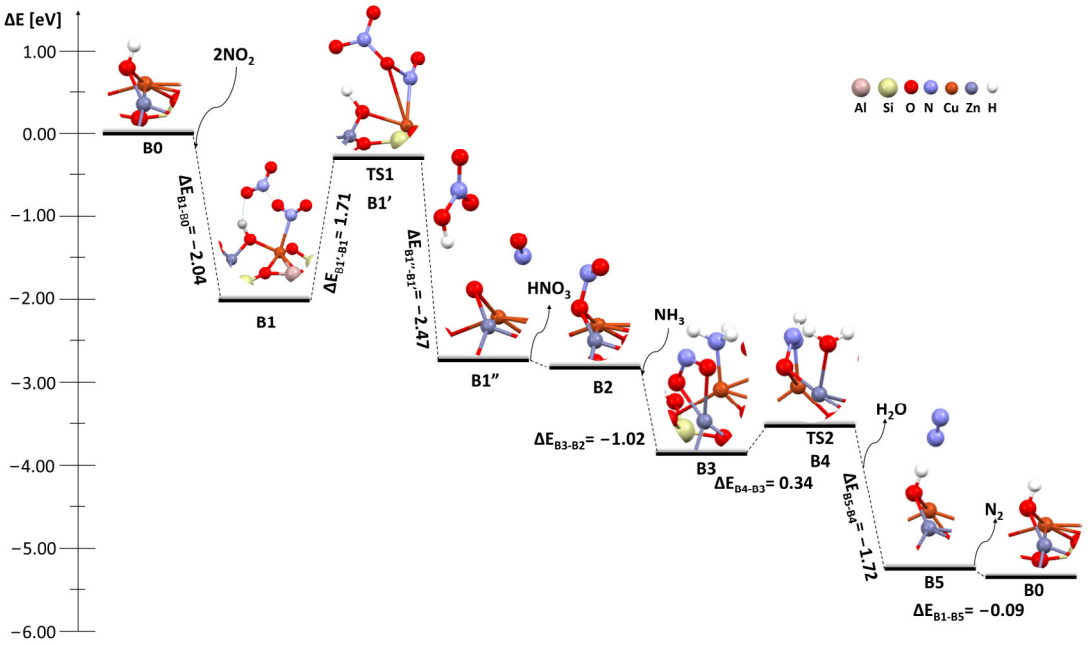

Figure 4. Energy diagram of the proposed mechanism of deNOx on the clinoptilolite zeolite with a bridged OH group in the dimer—Cu–O–Zn bimetallic dimer.

As mentioned earlier, the mechanism proposed by Bendrich et al. [11] was used, which, in the first step, allows the attachment of an NO molecule. Using the possibilities of the StoBe program, the two most relevant intermediate states were calculated. The first refers to the relatively complicated reaction of NO adsorption on the catalyst. First, with the release of energy, two NO_2 molecules are stabilised near the metal dimer (Figures 3(A1) and 4(B1)). This is followed by the formation of a complex that represents the first transition state in this mechanism (TS1-A1′ and TS1-B1′), obtained using the NEB method. Finally, there is a spontaneous detachment of the formed nitric acid(V) molecule, followed by the attachment of the leftover NO molecule. This process for both the Cu–O–Cu and Cu–O–Zn systems is strongly exothermic. The subsequent attachment of the reductant molecule, ammonia, is also exothermic. The barrier is lower for the copper complex (1.21 eV) in comparison to the Cu–O–Zn complex (1.71 eV). However, the Cu–O–Zn system attaches the NH_3 molecule more easily (see Figure 3(A3) or Figure 4(B3)). This is followed by the transformation, which is also endothermic (TS2-A4 or TS2-B4), and it represents a second important transition state. The transformation forms an imide group (-N_2H) and a water molecule. In the case of the Cu–O–Cu dimer, these intermediates are desorbed and located near the catalyst (Figure 3 (TS2-A4)). However, for the Cu–O–Zn dimer, both water and the imide group are adsorbed on the catalyst (Figure 4 (TS2-B4)). This is also represented in the energies that the system requires to form an intermediate state and then desorb the water molecule. For Cu–O–Zn, the transformation requires less energy because the products both stay on the surface (0.34 eV), while, for Cu–O–Cu, the amount of energy required to convert to products (which are attached to the catalyst) is higher (0.96 eV). Water is then desorbed from the system (as in the case of Cu–O–Cu; −2.85 eV) or from the surface of the dimer (as in the case of Cu–O–Zn; −1.72 eV). Because the water molecule in the system with two copper atoms already desorbs from the surface at the transformation stage, its removal is much more exothermic and therefore much easier. Next, N_2 desorption takes place, which is easier (exothermic) on Cu–O–Zn (compared to the endothermic process for the Cu–O–Cu system). Differences in the binding mode of the individual molecules, as well as transitions, are explained later.

Based on these mechanisms, we can conclude that the Cu–O–Zn bimetallic dimer is a slightly better catalyst for deNOx.

The next stage of the work consisted of carrying out the deNOx process for partially hydrated systems containing a hydroxyl group on one of the metal atoms (Figures 5 and 6). For the Cu–O–Zn system, both variants—OH on copper and OH on zinc—were considered.

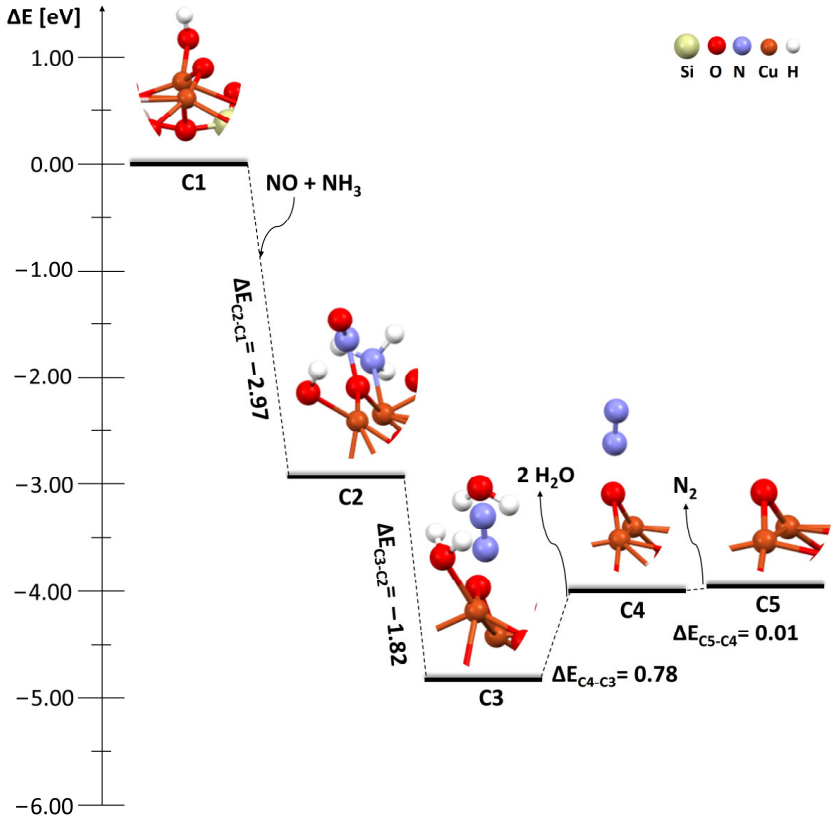

Figure 5. Energy diagram of the proposed mechanism of deNOx on the clinoptilolite zeolite with OH group on metal in the Cu–O–Cu monometallic dimer.

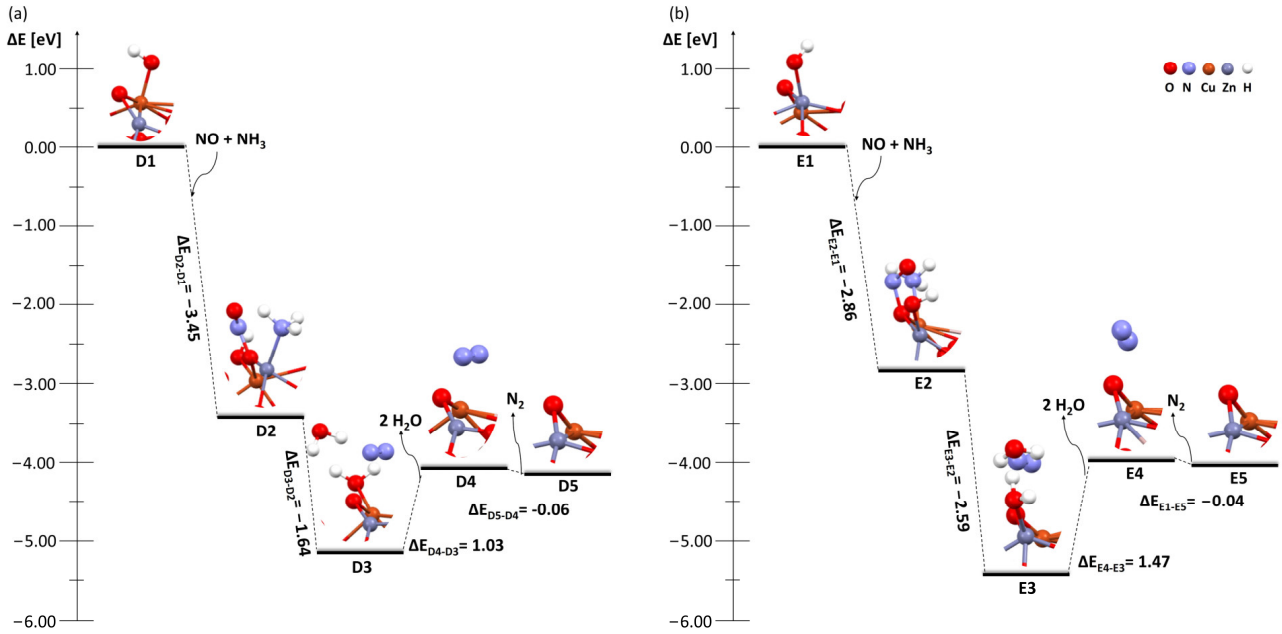

Figure 6. Energy diagram of the proposed mechanism of deNOx on the clinoptilolite zeolite with OH group on metal in the Cu–O–Zn bimetallic dimer: (**a**) OH group on Cu and (**b**) OH group on Zn.

For Cu–O–Cu systems, the direct coadsorption of NO and NH_3 was used without the participation of NO_2 or HNO_3 molecules (stages C1–C2). This type of approach worked well in previous studies [17]. In Figure 5, the attachment of nitric oxide and ammonia molecules can be seen to be strongly exothermic. In addition, the transformation process takes place with the release of energy to the environment (C2–C3). In the next step (C4), in contrast to in the previous systems, two water molecules are desorbed instead of one (one of them is formed by an OH group adsorbed on the metal). This stage is endothermic. Then, with almost no change in energy, the N_2 molecule is desorbed (C5), and the catalyst is ready to accept another OH group and regenerate for the deNOx process.

The same procedure was followed for the Cu–O–Zn system (Figure 6).

The presence of an OH group on a copper or zinc atom does not relatively change the behaviour of the catalyst (Figure 6). The same steps in either case are exothermic or endothermic. Only the amount of energy needed or released changes. Thus, in the system where the OH is located on copper, a much larger amount of energy is released to the environment during the attachment of NO and NH_3 (D1–D2) than in the structure with the OH group on zinc (E1–E2). In the transformation step, we have the completely opposite situation. The desorption of H_2O in both systems requires the addition of energy (less for the Cu–O–Cu system—D4), while the desorption of N_2 occurs with almost no change in energy (D5 and E5). Comparing the two systems with each other, we concluded that the one with the OH group on copper is slightly better. On the other hand, with respect to the previous monometallic system, it is the one with higher energy efficiency.

By comparing all the structures on which the deNOx process was carried out, it can be seen that the Cu–O–Zn bimetallic system with an OH group on bridged oxygen shows the best energy efficiency. In addition, when the OH group is adsorbed on copper, it also shows high efficiency. Unfortunately, by comparing the attached energy of the OH group to the metal atom in the bimetallic system (Figure 1), it can be seen that it has a slightly higher affinity for zinc.

2.3. *DeN_2O Mechanism*

Figure 7 presents a block diagram of the deN_2O process presented in this work. Figure 7a shows a schematic description of the deN_2O mechanism on a catalytic system containing a zeolite, dimer and an OH group on bridged oxygen. In this scheme, the first step is NO adsorption. Figure 7b represents a schematic visualisation of the deN_2O mechanism, where the first step is N_2O adsorption. The presence of hydrogen on the catalyst is not necessary here.

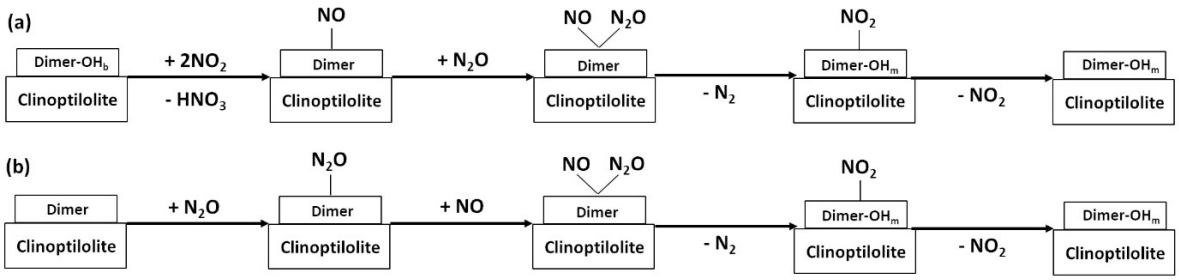

Figure 7. Schematic presentation of the deN_2O process on a clinoptilolite catalyst with a metal dimer: (**a**) dimer with an OH group on bridged oxygen which starts with NO, (**b**) dimer without an OH group (here, the OH it is not necessary) which starts with N_2O.

The next stage of the research consisted of carrying out the deN_2O process on pre-selected systems. Two approaches were analysed. In the first one, the NO molecule adsorbs first, followed by N_2O, while, in the second, the N_2O molecule adsorbs first, followed by NO. This order proved to be significant in the deN_2O process.

First, as before, the systems with an OH group on bridged oxygen were analysed (Figure 8).

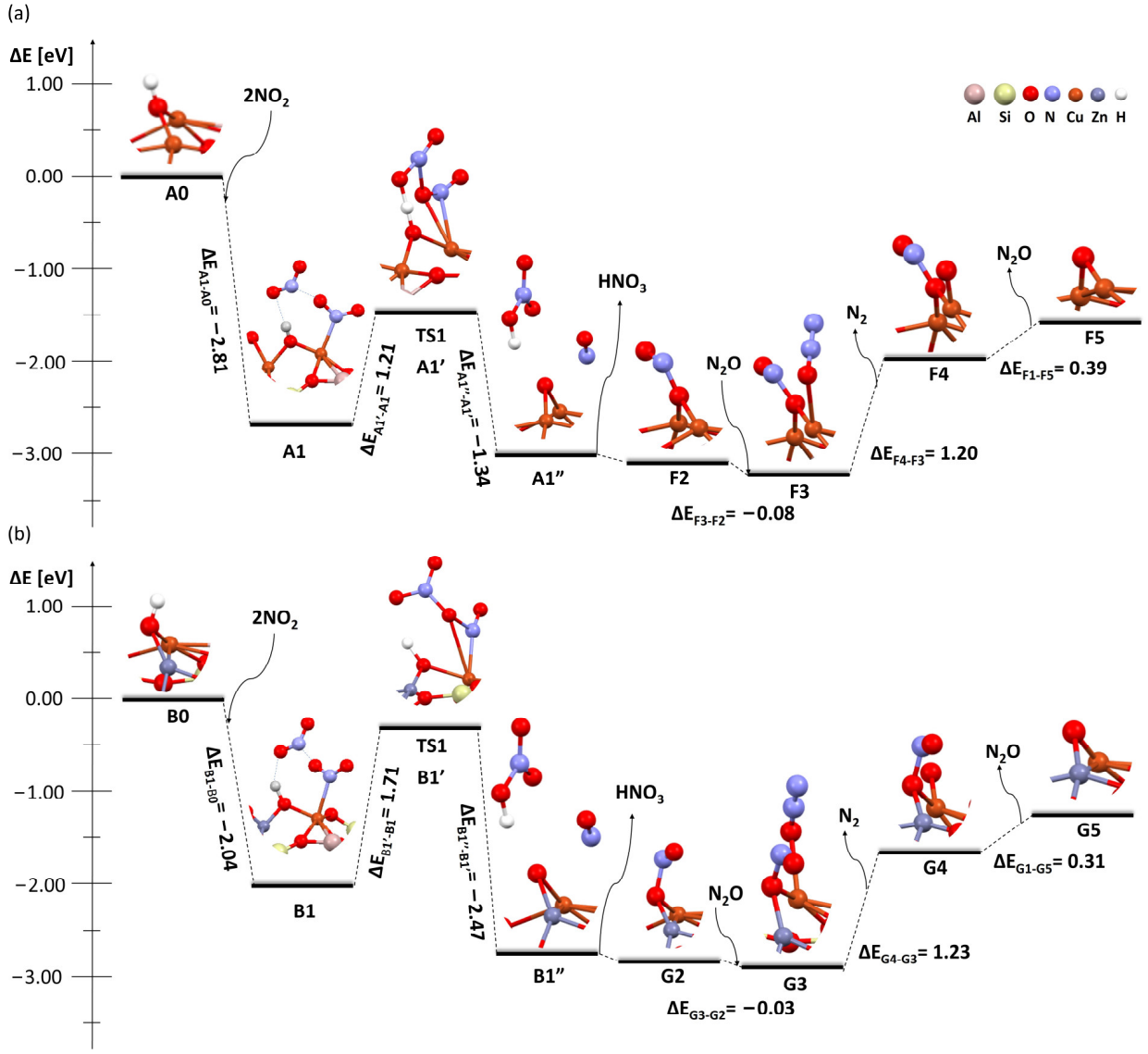

Figure 8. Energy diagram of the proposed mechanism of deN_2O (first step of NO adsorption) on the clinoptilolite zeolite with a bridged OH group in the dimer: (**a**) Cu–O–Cu monometallic dimer and (**b**) Cu–O–Zn bimetallic dimer.

Figure 8 presents the deN_2O process with the same first steps as the deNOx process (therefore, the symbols A and B are shown at the beginning of mechanisms). The adsorption of NO is then followed by the adsorption of an N_2O molecule (Figure 8a (F3) and 8b (G3)). In both cases, its adsorption is slightly exothermic. This is followed by a step in which the N_2 molecule is desorbed (F4 and G4). In both systems, this reaction is endothermic, and practically the same amount of energy is needed to release the nitrogen molecule. The last step is the desorption of NO_2 (F5 and G5), which is also endothermic, probably due to the distance of the oxygen from the NO molecule.

The deN_2O process for the same systems starting with the N_2O molecule (Figure 9) was then carried out.

A very important aspect is that N_2O does not attach to any of the atoms adsorbed on the zeolite surface. The nitrous oxide molecule does not affect the system, so the same steps as in the previous mechanism were followed. The analysis indicated that it is the presence of NO that allows the N_2O molecule drifting near the catalyst to attach (H1–H2 and I1–I2).

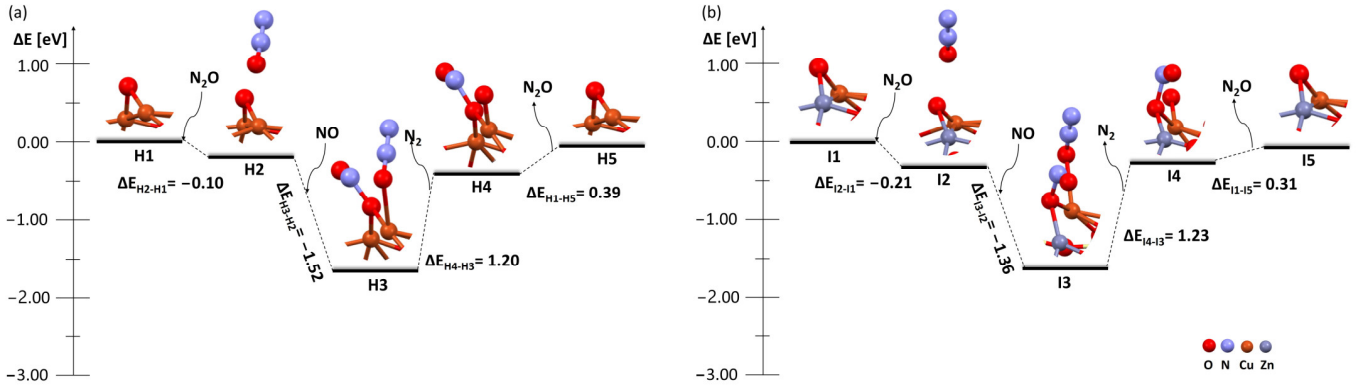

Figure 9. Energy diagram of the proposed mechanism of deN_2O (first step of N_2O adsorption) on the clinoptilolite zeolite with a bridged OH group in the dimer: (**a**) Cu–O–Cu monometallic dimer, and (**b**) Cu–O–Zn bimetallic dimer.

The same blocked scheme is also presented for the deN_2O mechanism on zeolite with a dimer and an OH group on one of the metal atoms (Figure 10). In this case, two approaches were also used—Figure 10a shows adsorption of NO as the first step, and Figure 10b shows the adsorption of N_2O as the first step.

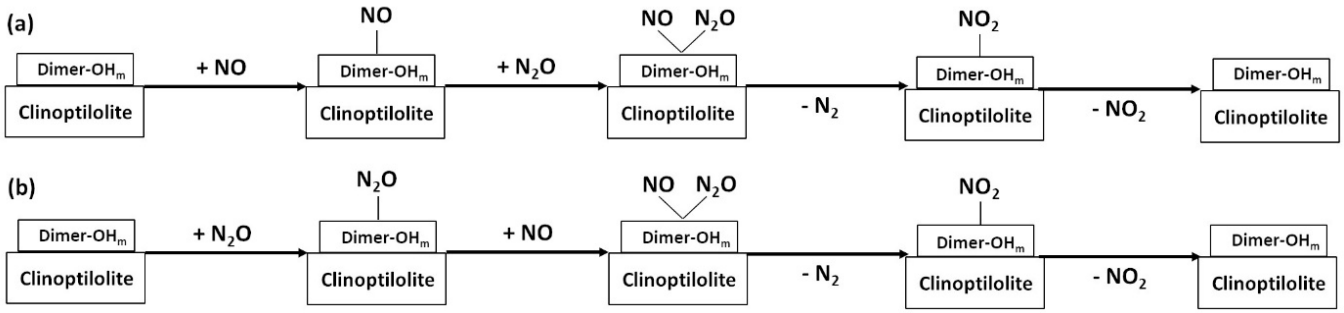

Figure 10. Schematic presentation of the deN_2O process on a clinoptilolite catalyst with a metal dimer and OH group on one of the metal atoms: (**a**) starts with NO, (**b**) starts with N_2O.

As mentioned before, the same process for a system with an OH group on one of the metals (Figures 11–13) was then carried out.

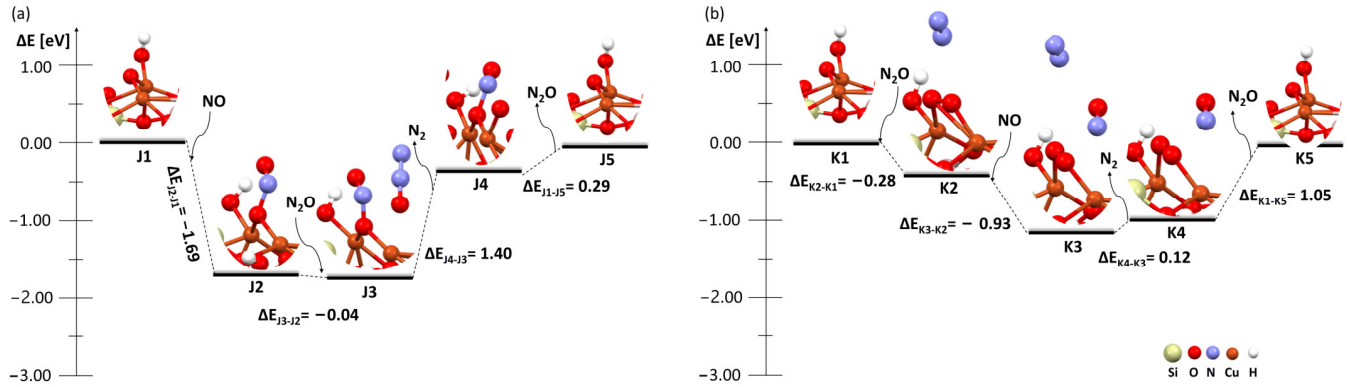

Figure 11. Energy diagram of the proposed mechanism of deN_2O on the clinoptilolite zeolite with OH group on metal in Cu–O–Cu monometallic dimer: (**a**) first step of NO and (**b**) first step of N_2O.

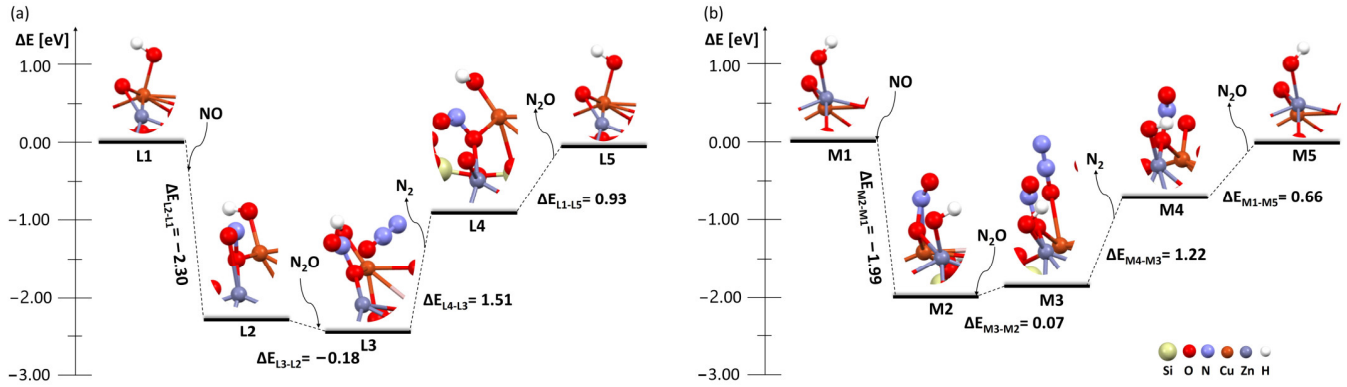

Figure 12. Energy diagram of the proposed mechanism of deN_2O (first step NO adsorption) on the clinoptilolite zeolite with an OH group on metal in the Cu–O–Zn bimetallic dimer: (**a**) OH group on Cu and (**b**) OH group on Zn.

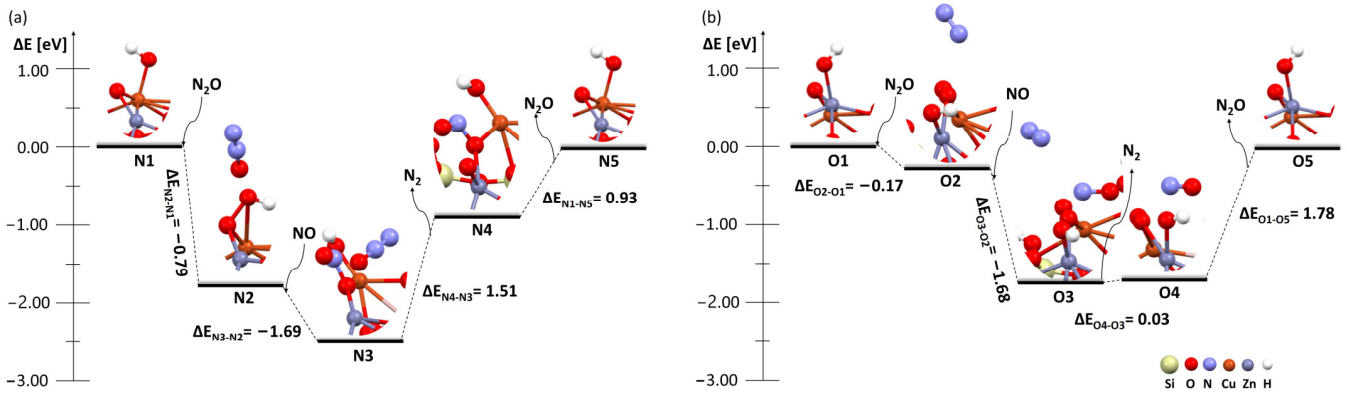

Figure 13. Energy diagram of the proposed mechanism of deN_2O (first step N_2O adsorption) on the clinoptilolite zeolite with an OH group on metal in the Cu–O–Zn bimetallic dimer: (**a**) OH group on Cu and (**b**) OH group on Zn.

Figure 11 shows the deN_2O process for the Cu–O–Cu system with an OH group on copper. The system behaves completely differently to when the OH group is on bridged oxygen. If NO adsorbs on the structure first, for N_2O, there is an attachment that significantly changes the structure of the system (J1–J2 and K1–K2). Coadsorption is not possible in either the first case (Figure 11a (J3)) or the second one (Figure 11b (K3)). With the addition of a second molecule, the energy of the system practically does not change. In both cases, further steps, such as the desorption of N_2 and NO_2, are endothermic (J4–J5 and K4–K5), but the first one is much more favourable when N_2O adsorbs first (it already forms the N_2 molecule detached from the system at the moment of adsorption) than in the situation when NO adsorbs first. The position of an OH group significantly affects the reaction mechanism.

The next two figures show this mechanism for the Cu–O–Zn system with an OH group on one of the metals. As shown in Figure 13, both when the OH group is located on the copper atom and on the zinc atom, NO attaches to the dimer (L1–L2 and M1–M2). The difference takes place in the next step, i.e., the adsorption of N_2O (L3 and M3). In the system with the OH group on copper, the N_2O molecule does not attach, in contrast to in the system with the OH group on zinc.

The presence of the OH group again influences the method of adsorption. In addition, in spite of the low energy needed for the attachment of N_2O to the system shown in Figure 12b, we can conclude that the subsequent steps—the N_2 desorption as well as the NO_2 desorption—occur more favourably than in the case of the system shown in Figure 12a.

The last mechanism analysed was deN_2O with N_2O adsorption at the beginning of the process (Figure 13).

In systems with a hydroxyl group on bridged oxygen, when the OH group is present on copper in a bimetallic system, N_2O does not attach (N1–N2 and O1–O2). The structure of the dimer changes, and there is a reduction in energy, even though the N_2O only drifts near the catalyst. The next steps were taken from previous calculations, as N_2O still does not form a bond with the catalyst when NO is added to the reaction system (N3 and O3). Things are different for the system with the OH group on zinc (Figure 14b). N_2O attaches, and the N_2 molecule detaches at the beginning of the reaction. On the other hand, when an NO molecule is added to the system, it significantly reduces its energy, but NO does not attach to the catalyst as it does after the N_2 desorption. Only the catalyst regeneration step and the desorption of the NO_2 molecule are strongly endothermic.

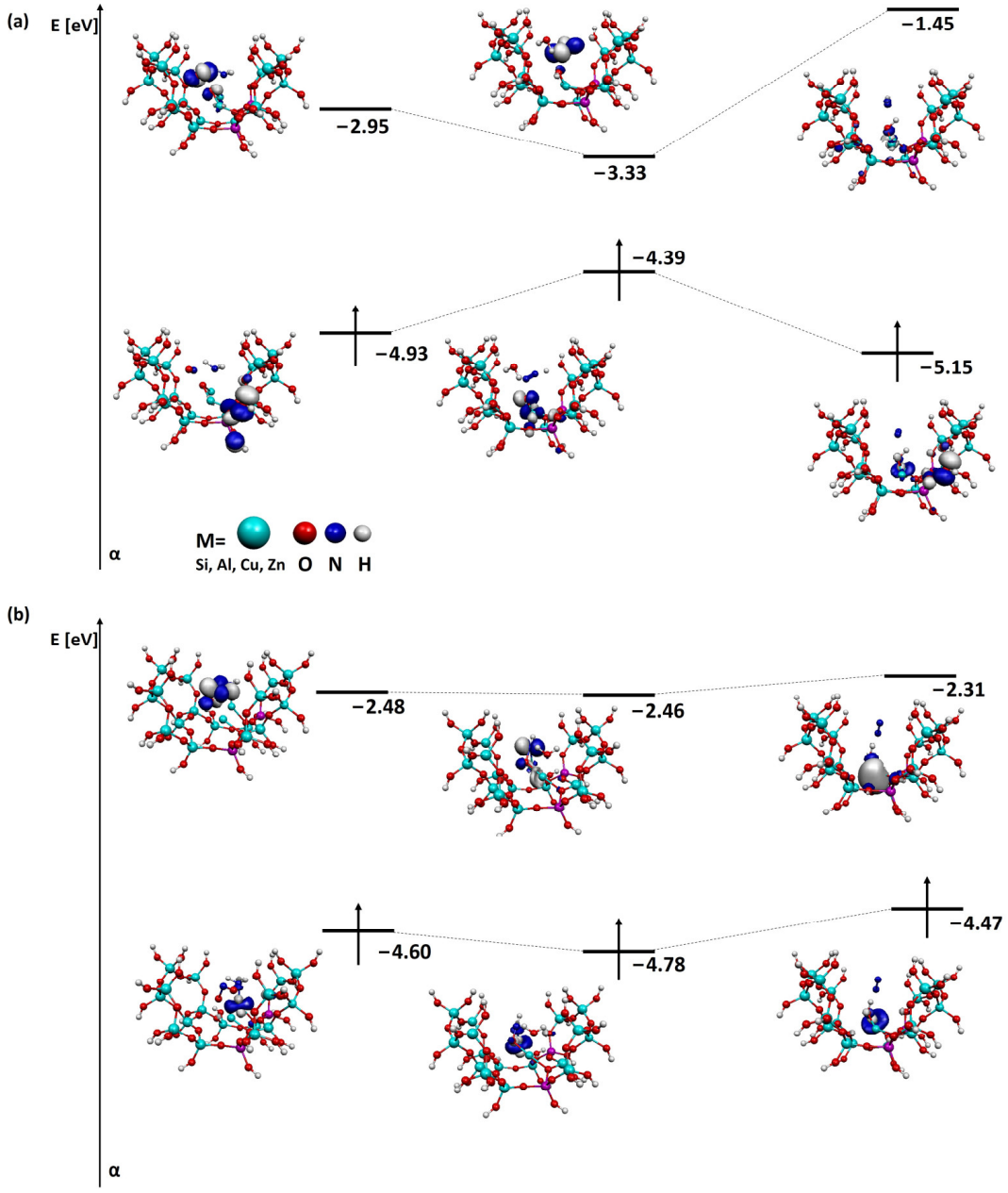

Figure 14. (**a**) SOMO and LUMO orbitals for the three most important steps in the deNOx mechanism for Cu–O–Cu with an OH group on bridged oxygen and (**b**) HOMO and LUMO orbitals for three important steps in the deNOx mechanism for Cu–O–Zn with an OH group on bridged oxygen.

Summarising all the mechanisms presented for the deN_2O process, the best system appears to be Cu–O–Cu with the OH group on copper, especially in the case where the N_2O adsorption occurs earlier. However, due to the high affinity of the catalytic system for NO, if such a catalyst is used in industry, it will have to be contacted first with an N_2O-containing gas and then with NO. The Cu–O–Zn bimetallic catalyst with the OH group on bridged oxygen proved equally interesting. In the case of this catalyst, the order of adsorbates does not matter, as N_2O only attaches after the NO attachment. Additionally, in the case of the deNOx process, this catalyst shows good energetic properties for the process.

Comparing all the collected information on the mechanism of the deNOx and deN_2O processes, the catalyst that is able to be used for both processes is a system with a bimetallic Cu–O–Zn dimer and a bridged OH group on clinoptilolite.

2.4. Molecular Orbitals

The final step of the analysis was the visualisation of the HOMO, SOMO and LUMO orbitals. Due to the different multiplicity of the systems (all energies are shown in Table S1 in the Supplementary Information), in some cases, we were dealing with HOMO orbitals (double filled for systems where there is no odd number of electrons or excitation states), SOMO orbitals (single-filled orbitals with the highest energy among the filled ones for systems where there is an odd number of electrons or excitation states) and LUMO orbitals (the first unfilled orbital with the lowest energy). The changes in orbitals for the three most relevant steps in the deNOx and deN_2O processes are shown below. For clarity of the analysis, only the system containing the OH group on bridged oxygen was selected for comparison due to the fact that the previous analyses indicated that it is the Cu–O–Zn bimetallic catalyst with the OH group on bridged oxygen that shows the most promising properties for nitrogen industrial processes. Analyses of the orbitals of the other structures are presented in the Supplementary Information (Figures S3–S6).

Figure 14 shows the orbitals for structures with an OH group on bridged oxygen for the Cu–O–Cu system (Figure 14a) and for the Cu–O–Zn system (Figure 14b).

The difference related to the energy of the individual orbitals in a given system is the most important. As shown in Figure 14b, the energy of the SOMO orbital first increases, then decreases, while the opposite behaviour is observed for the LUMO orbital for this system. Its energy first decreases and then increases significantly. In contrast, the Cu–O–Zn structure (Figure 14b) shows that the energy change for both the HOMO and LUMO orbitals is not significant. Additionally, in the case of the Cu–O–Cu structure, it is visible that the location of the orbitals also changes. Only the central system shows that the orbital is located close to the atoms of the metal dimer. On the other hand, in the case of the Cu–O–Zn system, both the HOMO and SOMO orbitals are located close to the metal dimer. The location of the LUMO orbital on the metallic dimer in the Cu–O–Zn structure confirms that this system is transformed more easily and participates in the deNOx process.

The SOMO and LUMO orbitals were then analysed for the deN_2O process on the Cu–O–Cu system with an OH group on bridged oxygen (Figure 15).

A significant reduction in the energy of the LUMO atom, where the N_2O molecule adsorbs first on the system, was observed. Similarly, the final energy of the SOMO orbital decreases. This confirms previous analyses showing that beginning the adsorption from the N_2O molecule results in an easier deN_2O process. The system always moves to a lower energy. The second characteristic of this system is that, when starting the adsorption from both NO and N_2O, the SOMO orbital is located on the zeolite, while LUMO is located on the metallic dimer.

The orbitals for the Cu–O–Zn system with an OH group on bridged oxygen were analysed finally (Figure 16). A strong similarity to the deN_2O process on the Cu–O–Cu system with an OH group on bridged oxygen was noted.

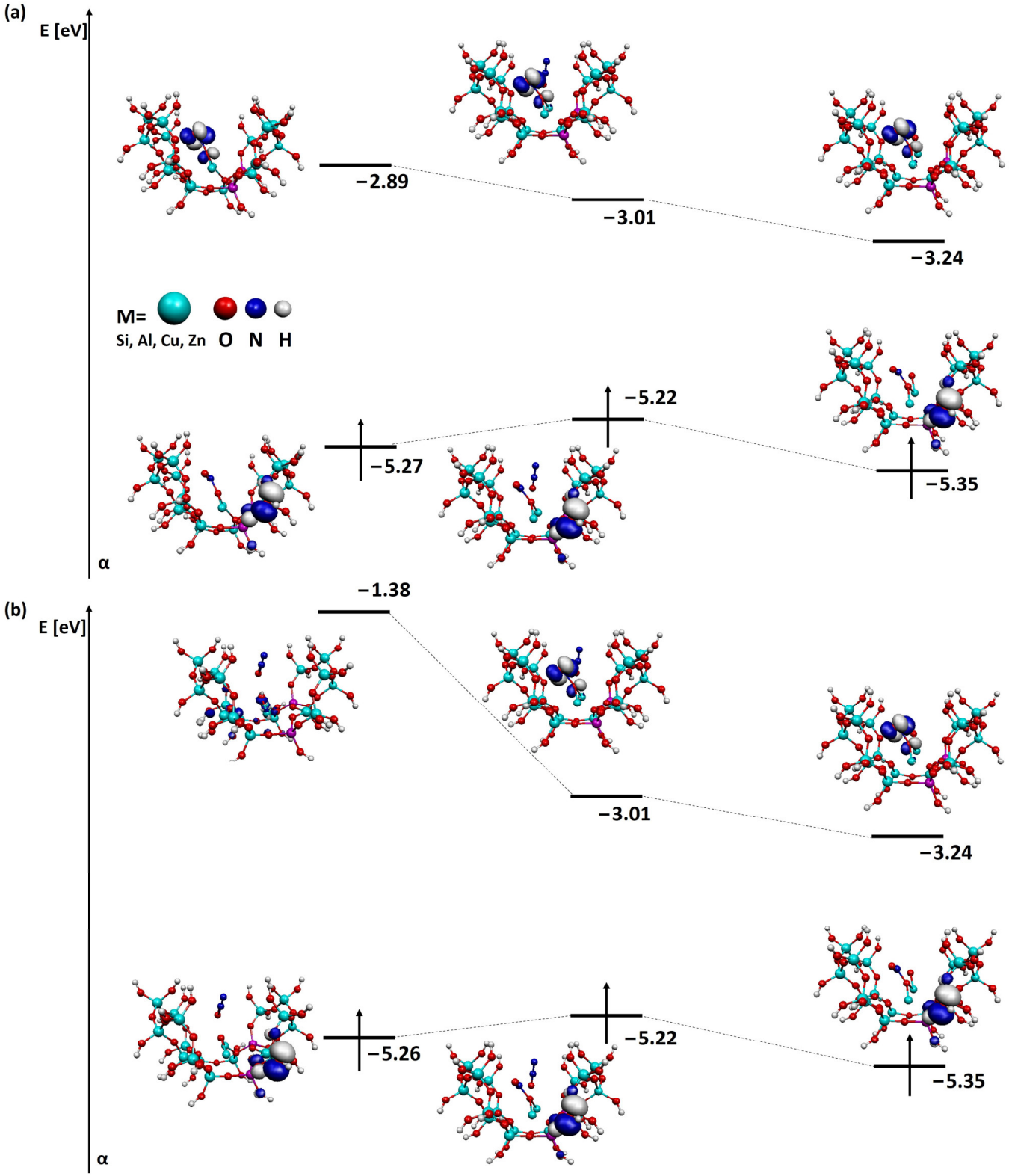

Figure 15. SOMO and LUMO orbitals for the three most important steps in the deN_2O mechanism for Cu–O–Cu with an OH group on bridged oxygen: (**a**) starts with NO; (**b**) starts with N_2O.

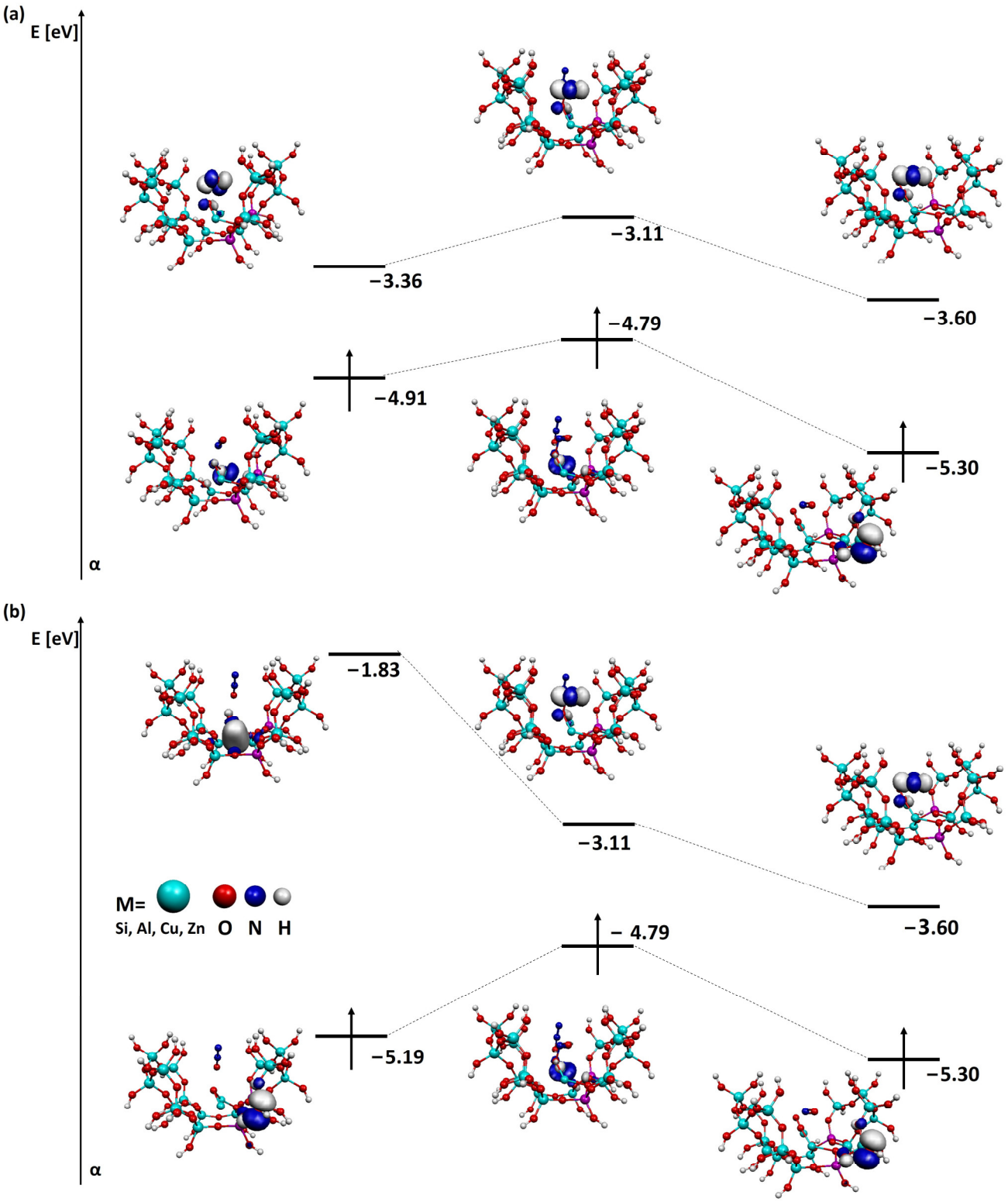

Figure 16. SOMO and LUMO orbitals for the three most important steps in the deN_2O mechanism for Cu–O–Zn with an OH group on bridged oxygen: (**a**) starts with NO; (**b**) starts with N_2O.

In both cases, starting from both the NO molecule (Figure 16a) and the N_2O molecule (Figure 16b), the last step is characterised by the reduced energy of the SOMO and LUMO orbitals. In the case of the N_2O adsorption as the first molecule, the reduction in the energy

of the LUMO orbital is significant. In addition, similarly to the previous system, the SOMO orbitals are located on zeolite, while the LUMO orbitals are located on the metallic dimer.

2.5. Electron Analysis

A full ionicity and electron analysis is presented in the Supplementary Information (Figures S7–S21).

3. Discussion

Putting together the analyses of the orbitals for the presented systems, it was observed that they confirm previous conclusions, i.e., the most favourable catalytic system for both deNOx and deN_2O processes is the Cu–O–Zn bimetallic system with an OH group on bridged oxygen, and starting the deN_2O process from the N_2O molecule increases the efficiency of the deN_2O process. In the deNOx process, when it takes place on a catalytic system where the hydroxyl group is located on a bridged oxygen, the -N_2H intermediate mentioned in the literature [60] is formed (Figure S15). As expected, the formation of this intermediate is the limiting step (energy input to the system is needed to form it) (Figures 3 and 4). However, in the case of the Cu–O–Zn bimetallic dimer, this energy is lower, showing that the presence of zinc in the dimer can improve the efficiency of the deNOx process.

Looking globally at the calculations and analyses carried out, we also observed several regularities for the deN_2O process. The main aspect is the order of adsorption of NO and N_2O, which has a significant influence on the further paths of the mechanism. In the dimers without an OH group on one of the metals, the N_2O molecule adsorbs on the catalyst surface only when a NO molecule is present in the reaction environment. This shows that the dimer alone, without interaction with NO, is unable to affect N_2O decomposition (Figures S17 and S18). This was also confirmed in the analysis of the orbitals, where NO forms the LUMO orbital, which is reactive (Figure 15).

If, on the other hand, we consider dimers with a hydroxyl group on one of the metals, it can be observed that Zn does not have a very significant effect on the limiting step, which is the desorption of the N_2 molecule. Only in the case of a bimetallic dimer with an OH group on zinc and N_2O adsorption first does this step have a significantly reduced energy barrier.

However, the deN_2O process carried out on a Cu–O–Zn bimetallic system with an OH group on bridged oxygen is relatively efficient and can occur regardless of the order of NO or N_2O adsorption.

It is also interesting to note that, in the case of NO and NH_3 adsorption on the Cu–O–Zn system, the dimer structure is disrupted at one of the stages (Figure S15), contrary to the literature report of increased catalyst stability upon Zn addition. Further studies of this system may provide an explanation for this difference. One more thing to present is a comparison of the results obtained with previous studies. A comparison with the mechanism of the deNOx process carried out on FAU and MFI zeolites with Cu–O–Zn bimetallic dimer is deserving of special attention [15]. In the case of the FAU zeolite, the energy barrier of the limiting step (formation of -N_2H) is 0.45 eV, while, for the MFI zeolite, it is equal to 0.75. We can confidently state that our calculations prove that the clinoptilolite with Cu–O–Zn dimer is more efficient in the deNOx process, because the energy barrier of the limiting step is 0.34 eV.

4. Experimental

4.1. Computational Details

The ab initio density functional theory (DFT) method was used to calculate the electron structure of the presented clusters with StoBe software (http://www.fhi-berlin.mpg.de/KHsoftware/StoBe/ (accessed on 8 August 2023)) [66]. The exchange and correlation functional was approximated with a Perdew–Burke–Ernzerhof (PBE) functional [67,68]. It was used for electron exchange and correlation. By linear combinations of atomic orbitals

(LCAO) and using conventional Gaussian basis sets for atoms, Kohn–Sham orbitals were presented [69].

Mulliken populations [70] and Mayer's bond order factors [71,72] were used to precisely analyse the electron structure of the clusters. Molecular orbitals were also analysed. Visualisations were presented with the Molekel program [65].

Double-zeta valence polarisation (DZVP) functional bases were used for orbital basis sets Si and Al (6321/521/1), Cu and Zn (63321/531/311), O and N (621/41/1) and H (41). Additionally, auxiliary functional bases were used to adjust the electron density and the exchange potential of the correlation of individual atoms: Si and Al (5,4;5,4), Cu and Zn (5,5;5,5), O and N (4,3;4,3) and H (4,0;4,0).

The NEB parameter in StoBe software was used to determine the structure and energy of the transition state. This keyword defines control parameters of a reaction path optimisation using the nudged elastic band (NEB) method (see C1), where both the standard NEB [73–75] and the climbing image NEB (CI-NEB) approach [76] were implemented. The quasi-Newton Broyden–Fletcher–Goldfarb–Shanno variant was used for the local optimisation and path extrapolation method used in the NEB path optimization. The 0.5 and 0.1 spring constants (R×8 values) for the basic spring constant and the variation of the spring constant for the lowest images, respectively, were used in the elastic coupling between adjacent images along the NEB reaction path.

4.2. Geometrical Models

The structure for calculations was taken from [77,78] (Figure 1). A single crystal unit cell contains 197 atoms, a cubic phase of clinoptilolite zeolite framework type is characterised by the monoclinic space group C 1 2/m 1 (# 12) with a lattice constant of a = 17.52 Å, b = 17.64 Å and c = 7.40 Å, and $\alpha = \gamma = 90°$, and $\beta = 116.104°$.

To create a cluster for the calculation, a section containing the most important five T-points was cut out. The structure of the obtained cluster was as follows: $Si_{18}O_{50}H_{30}$ (Figure 17). The broken bonds were saturated with a single positive charge—a hydrogen atom. The distance of the oxygen atom to the hydrogen was 0.97, and the direction was in line with that of the removed atom. For analyses related to catalytic reactions, aluminium atoms were introduced into the system, as proposed by Uzunova and Mikosch [79]. The results of the calculations can be seen in the Supplementary Information. The most energetically favourable system was selected for further analyses (Figure S22).

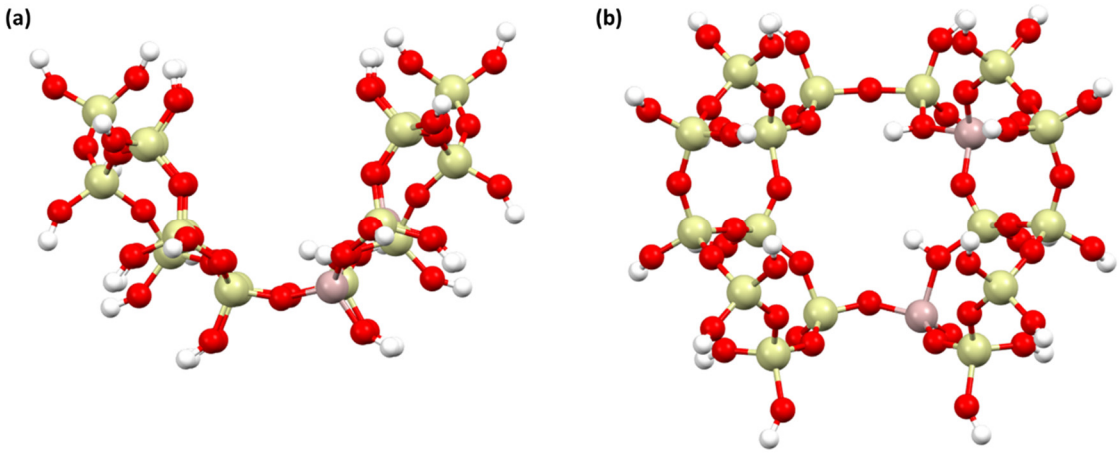

Figure 17. Cluster model of clinoptilolite zeolite structure $Al_2Si_{16}O_{50}H_{30}$: (**a**) view along (100) and (**b**) view along (001). The colour of the atoms: pink—aluminium, yellow—silica, red—oxygen, white—hydrogen.

5. Conclusions

Summarising the calculations and analyses carried out, we can come to certain conclusions. The presence of water in the reaction system can have a beneficial effect on the

catalyst by facilitating the formation of bridging OH groups or the attachment of OH groups to metal atoms in the dimer. The location of the OH group influences the behaviour of the catalytic system, changing the different steps in the process, as well as the number of end products (one water molecule when the OH group is on bridged oxygen or two water molecules when the OH group is on one of the metals in the dimer).

Catalytic systems appear to be more favourable energetically when N_2O is first adsorbed onto the surface, but this is difficult to achieve due to the high affinity of NO for the system. An industrial solution could be to introduce a gas containing N_2O and then NO onto the catalyst. However, in some catalytic systems, such as Cu–O–Cu and Cu–O–Zn with an OH group on bridged oxygen, the sequence of molecules does not matter, as N_2O only attaches after NO adsorbs into the system. From the analysis of the reaction mechanisms for the deNOx process, the most energy-efficient catalyst is the Cu–O–Zn bimetallic dimer system with an OH group on bridged oxygen, while, for the deN_2O process, it is the Cu–O–Cu monometallic system with an OH group on the copper atom and preadsorption of N_2O. However, due to the fact that it may be difficult to obtain N_2O adsorption first for the latter system, we can conclude from the comparisons that the best catalyst for the deNOx process, i.e., Cu–O–Zn with a bridged OH group, is also very effective for the deN_2O process.

Supplementary Materials: The following supporting information can be downloaded at: https://www.mdpi.com/article/10.3390/catal13081210/s1, Figure S1: Bond order and length (in brackets) for zeolite clinoptilolite structures: (a) Cu-O-Cu dimer with OH group on copper, (b) Cu-O-Zn dimer with OH group on copper, (c) Cu-O-Zn dimer with OH group on zinc and ionicity for: (d) Cu-O-Cu dimer with OH group on copper, (e) Cu-O-Zn dimer with OH group on copper, (f) Cu-O-Zn dimer with OH group on zinc; Figure S2: Bond order and lenght (in brackets) for zeolite clinoptilolite structures: (a) Cu-O-Cu dimer with OH group on oxygen bridge, (b) Cu-O-Zn dimer with OH group on oxygen bridge and ionicity: (c) Cu-O-Cu dimer with OH group on oxygen bridge, (d) Cu-O-Zn dimer with OH group on oxygen bridge; Figure S3: SOMO and LUMO orbitals for three most important steps in deNOx mechanism for (a) Cu-O-Cu with OH group on copper; (b) for Cu-O-Zn with OH group on copper and (c) for Cu-O-Zn with OH group on zinc; Figure S4: SOMO and LUMO orbitals for three most important steps in deN_2O mechanism for Cu-O-Cu with OH group on copper: (a) starts with NO; (b) starts with N_2O; Figure S5: SOMO and LUMO orbitals for three most important steps in deN_2O mechanism for Cu-O-Zn with OH group on copper: (a) starts with NO; (b) starts with N_2O; Figure S6: SOMO and LUMO orbitals for three most important steps in deN_2O mechanism for Cu-O-Zn with OH group on zinc: (a) starts with NO; (b) starts with N_2O; Table S1: Energies for different structure and considered multiplicities for deNOx process; Table S2: Energies for different structure and considered multiplicities for deN_2O process; Figure S7: Ionicity for zeolite clinoptilolite structures from deNOx process: dimer Cu-O-Cu with OH group on bridged oxygen—(a) step A3, (b) step A4, (c) step A5; dimer Cu-O-Zn with OH group on bridged oxygen—(d) step B3, (e) step B4, (f) step B5; Figure S8: Ionicity for zeolite clinoptilolite structures from deNOx process: dimer Cu-O-Cu with OH group on copper—(a) step C2, (b) step C3, (c) step C4; dimer Cu-O-Zn with OH group on copper—(d) step D2, (e) step D3, (f) step D4 and dimer Cu-O-Zn with OH group on zinc—(g) step E2, (h) step E3 and (i) step E4; Figure S9: Ionicity for zeolite clinoptilolite structures from deN_2O process: dimer Cu-O-Cu with OH group on copper—(a) step F2, (b) step H2, (c) step F3 (H3), (d) step F4 (H4); Figure S10: Ionicity for zeolite clinoptilolite structures from deN_2O process: dimer Cu-O-Zn with OH group on bridged oxygen– (a) step G2, (b) step I2, (c) step G3 (I3), (d) step G4 (I4); Figure S11: Ionicity for zeolite clinoptilolite structures from deN_2O process: dimer Cu-O-Cu with OH group on copper—(a) step J2, (b) step J3, (c) step J4 when NO is first, (d) step K2, (e) step K3 and (f) step K4 when N_2O is first; Figure S12: Ionicity for zeolite clinoptilolite structures from deN_2O process: dimer Cu-O-Zn with OH group on copper—(a) step L2, (b) step N2, (c) step L3 (N3) and (d) step L4 (N4); Figure S13: Ionicity for zeolite clinoptilolite structures from deN_2O process: dimer Cu-O-Zn with OH group on zinc—(a) step M2, (b) step M3, (c) step M4 when NO is first, (d) step O2, (e) step O3 and (f) step O4 when N_2O is first; Figure S14: Bond order and length (in brackets) for the zeolite clinoptilolite structures from two molecule NO2 adsorption: (a) step A1 (see Figure 4), (b) step B1 (see Figure 4); Figure S15: Bond order and length (in brackets) for the zeolite clinoptilolite structures from deNOx process: dimer Cu-O-Cu with OH group on bridged oxygen—(a) step A3,

(b) step A4, (c) step A5; dimer Cu-O-Zn with OH group on bridged oxygen—(d) step B3, (e) step B4, (f) step B5; Figure S16: Bond order and length (in brackets) for the zeolite clinoptilolite structures from deNOx process: dimer Cu-O-Cu with OH group on copper—(a) step C2, (b) step C3, (c) step C4; dimer Cu-O-Zn with OH group on copper—(d) step D2, (e) step D3, (f) step D4 and dimer Cu-O-Zn with OH group on zinc— (g) step E2, (h) step E3, and (i) step E4; Figure S17: Bond order and length (in brackets) for the zeolite clinoptilolite structures from deN_2O process: dimer Cu-O-Cu with OH group on bridged oxygen—(a) step F2, (b) step H2, (c) step F3 (H3), (d) step F4 (H4); Figure S18: Bond order and length (in brackets) for zeolite clinoptilolite structures from deN_2O process: dimer Cu-O-Zn with OH group on bridged oxygen– (a) step G2, (b) step I2, (c) step G3 (I3), (d) step G4 (I4); Figure S19: Bond order and length (in brackets) for the zeolite clinoptilolite structures from deN_2O process: dimer Cu-O-Cu with OH group on copper—(a) step J2, (b) step J3, (c) step J4 when NO is first, (d) step K2, (e) step K3 and (f) step K4 when N_2O is first; Figure S20: Bond order and length (in brackets) for the zeolite clinoptilolite structures from deN_2O process: dimer Cu-O-Zn with OH group on copper—(a) step L2, (b) step N2, (c) step L3 (N3) and (d) step L4 (N4); Figure S21: Bond order and length (in brackets) for the zeolite clinoptilolite structures from deN_2O process: dimer Cu-O-Zn with OH group on zinc—(a) step M2, (b) step M3, (c) step M4 when NO is first, (d) step O2, (e) step O3 and (f) step O4 when N_2O is first; Figure S22: Clinoptilolite structure with two aluminium atom in different T-position with ex-change energy below structure: (a) aluminium on T1-T1, (b) aluminium on T1-T2, (c) aluminium on T2-T3 and (d) aluminium on T3 and T3.

Author Contributions: Conceptualisation, I.K. and I.C.; Formulation of the scientific problem and development of theoretical part, I.K. and I.C.; Methodology, I.K. and I.C.; Investigation, I.K. and W.M.; Data curation, validation and visualisation, I.K. and W.M.; Writing—original draft, I.K. and W.M.; Supervision and writing—review and editing, I.C. All authors have read and agreed to the published version of the manuscript.

Funding: This article is the effect of the realization of the project plgzeodesign2023 at Poland's high-performance computing infrastructure PLGrid.

Data Availability Statement: Data is contained within the article.

Acknowledgments: We gratefully acknowledge Poland's high-performance computing infrastructure PLGrid (HPC Centers: ACK Cyfronet AGH, WCSS, CI TASK) for providing computer facilities and support within computational grant no. PLG/2023/016153.

Conflicts of Interest: The authors declare no conflict of interest.

References

1. Zhang, J.; Liang, J.; Peng, H.; Mi, Y.; Luo, P.; Xu, H.; He, M.; Wu, P. Cost-effective fast-synthesis of chabazite zeolites for the reduction of NO_x. *Appl. Catal. B* **2021**, *292*, 120163. [CrossRef]
2. Yan, R.; Lin, S.; Li, Y.; Liu, W.; Mi, Y.; Tang, C.; Wang, L.; Wu, P.; Peng, H. Novel shielding and synergy effects of Mn-Ce oxides confined in mesoporous zeolite for low temperature selective catalytic reduction of NO_x with enhanced SO_2/H_2O tolerance. *J. Hazard. Mater.* **2020**, *396*, 122592. [CrossRef] [PubMed]
3. Liang, J.; Mi, Y.; Song, G.; Peng, H.; Li, Y.; Yan, R.; Liu, W.; Wang, Z.; Wu, P.; Liu, F. Environmental benign synthesis of Nano-SSZ-13 via FAU transcrystallization: Enhanced NH_3-SCR performance on Cu-SSZ-13 with nanosized effect. *J. Hazard. Mater.* **2020**, *398*, 122986. [CrossRef] [PubMed]
4. Chlebda, D.K.; Stachurska, P.; Jędrzejczyk, R.J.; Kuterasiński, Ł.; Dziedzicka, A.; Górecka, S.; Chmielarz, L.; Łojewska, J.; Sitarz, M.; Jodłowski, P.J. DeNOx Abatement over Sonically Prepared Iron-Substituted Y, USY and MFI Zeolite Catalysts in Lean Exhaust Gas Conditions. *J. Nanomater.* **2018**, *8*, 21. [CrossRef]
5. Lammel, G.; Graßl, H. Greenhouse effect of NO_x. *Environ. Sci. Pollut. Res.* **1995**, *2*, 40–45. [CrossRef]
6. Inger, M.; Moszowski, B.; Ruszak, M.; Rajewski, J.; Wilk, M. Two-Stage Catalytic Abatement of N_2O Emission in Nitric Acid Plants. *Catalysts* **2020**, *10*, 987. [CrossRef]
7. Ho, P.H.; Jabłońska, M.; Palkovits, R.; Rodríguez-Castellón, E.; Ospitali, F.; Fornasari, G.; Vaccari, A.; Benito, P. N_2O catalytic decomposition on electrodeposited Rh-based open-cell metallic foams. *J. Chem. Eng.* **2020**, *379*, 122259. [CrossRef]
8. Basahel, S.N.; Mokhtar, M.; Ali, T.T.; Narasimharao, K. Porous Fe_2O_3-ZrO_2 and NiO-ZrO_2 nanocomposites for catalytic N_2O decomposition. *Catal. Today* **2020**, *348*, 166–176. [CrossRef]
9. Li, M.; Zhang, R.; Wang, H.; Chen, H.; Wei, Y. Role of the exposure facets upon diverse morphologies of cobalt spinels on catalytic deN_2O process. *Catal. Today* **2021**, *376*, 177–187. [CrossRef]
10. Chen, P.; Rizzotto, V.; Khetan, A.; Xie, K.; Moos, R.; Pitsch, H.; Ye, D.; Simon, U. Mechanistic Understanding of Cu-CHA Catalyst as Sensor for Direct NH_3-SCR Monitoring: The Role of Cu Mobility. *ACS Appl. Mater. Interfaces* **2019**, *11*, 8097–8105. [CrossRef]

11. Bendrich, M.; Scheuer, A.; Hayes, R.E.; Votsmeier, M. Unified mechanistic model for Standard SCR, Fast SCR, and NO_2 SCR over a copper chabazite catalyst. *Appl. Catal. B Environ.* **2018**, *222*, 76–87. [CrossRef]
12. Shan, W.; Yu, Y.; Zhang, Y.; He, G.; Peng, Y.; Li, J.; He, H. Theory and practice of metal oxide catalyst design for the selective catalytic reduction of NO_x with NH_3. *Catal. Today* **2021**, *376*, 292–301. [CrossRef]
13. Pankin, I.A.; Hamoud, H.I.; Lomachenko, K.A.; Rasmussen, S.B.; Martini, A.; Bazin, P.; Valtchev, V.; Maturi, M.; Lamberti, C.; Bordiga, S. Cu- and Fe-speciation in composite zeolite catalyst for selective catalytic reduction of NO_x: Insights from operando XAS. *Catal. Sci. Technol.* **2021**, *11*, 846–860. [CrossRef]
14. Guan, B.; Jiang, H.; Wei, Y.; Liu, Z.; Wu, X.; Lin, H.; Huang, Z. Density functional theory researches for atomic structure, properties prediction, and rational design of selective catalytic reduction catalysts: Current progresses and future perspectives. *Mol. Catal.* **2021**, *510*, 111704. [CrossRef]
15. Kurzydym, I.; Czekaj, I. Theoretical studies on the mechanism of deNOx process in Cu-Zn bimetallic system—Comparison of FAU and MFI zeolites. *Molecules* **2022**, *27*, 300. [CrossRef] [PubMed]
16. Kurzydym, I.; Czekaj, I. Theoretical studies of SCR deNOx over Cu-, Mn- and Fe-FAU catalysts. *Chem. Chem. Technol.* **2021**, *15*, 16–25. [CrossRef]
17. Jodłowski, P.J.; Czekaj, I.; Stachurska, P.; Kuterasiński, Ł.; Chmielarz, L.; Jędrzejczyk, R.J.; Jeleń, P.; Sitarz, M.; Górecka, S.; Mazur, M.; et al. Experimental and Theoretical Studies of Sonically Prepared Cu-Y, Cu-USY and Cu-ZSM-5 Catalysts for SCR deNOx. *Catalysts* **2021**, *11*, 824. [CrossRef]
18. Endou, A.; Jung, C.; Kusagaya, T.; Kubo, M.; Selvam, P.; Miyamoto, A. Combinatorial computational chemistry approach to the design of metal catalysts for deNOx. *Appl. Surf. Sci.* **2004**, *223*, 159–167. [CrossRef]
19. Ye, B.; Jeong, B.; Lee, M.J.; Kim, T.H.; Park, S.S.; Jung, J.; Lee, S.; Kim, H.D. Recent trends in vanadium-based SCR catalysts for NOx reduction in industrial applications: Stationary sources. *Nano Converg.* **2022**, *9*, 51. [CrossRef]
20. Huang, L.; Zeng, Y.; Gao, Y.; Wang, H.; Zong, Y.; Chang, Z.; Zhang, S.; Han, P.; Yu, Y. Promotional effect of phosphorus addition on improving the SO_2 resistance of V_2O_5-MoO_3/TiO_2 catalyst for NH_3-SCR of NO. *J. Phys. Chem. Solids* **2022**, *163*, 110566. [CrossRef]
21. Xin, Y.; Li, Q.; Zhang, Z. Zeolitic Materials for DeNOx Selective Catalytic Reduction. *ChemCatChem* **2018**, *10*, 29–41. [CrossRef]
22. Wang, P.; Yu, D.; Zhang, L.; Ren, Y.; Jin, M.; Lei, L. Evolution mechanism of NO_x in NH_3-SCR reaction over Fe-ZSM-5 catalyst: Species-performance relationships. *Appl. Catal. A Gen.* **2020**, *607*, 117806. [CrossRef]
23. Zeng, J.; Chen, S.; Fan, Z.; Wang, C.; Chang, H.; Li, J. Simultaneous Selective Catalytic Reduction of NO and N_2O by NH_3 over Fe-Zeolite Catalysts. *Ind. Eng. Chem. Res.* **2020**, *59*, 19500–19509. [CrossRef]
24. Khivantsev, K.; Kwak, J.-H.; Jaegers, N.R.; Koleva, I.Z.; Vayssilov, G.N.; Derewinski, M.A.; Wang, Y.; Aleksandrov, H.A.; Szanyi, J. Identification of the mechanism of NO reduction with ammonia (SCR) on zeolite catalysts. *Chem. Sci.* **2022**, *13*, 10383–10394. [CrossRef] [PubMed]
25. Shan, Y.; Du, J.; Zhang, Y.; Shan, W.; Shi, X.; Yu, Y.; Zhang, R.; Meng, X.; Xiao, F.-S.; He, H. Selective catalytic reduction of NO_x with NH_3: Opportunities and challenges of Cu-based small-pore zeolites. *Natl. Sci. Rev.* **2021**, *8*, nwab010. [CrossRef] [PubMed]
26. Ghasemian, N.; Falamaki, C. Zn^{2+}, Fe^{2+}, Cu^{2+}, Mn^{2+}, H^+ Ion-exchanged and Raw Clinoptilolite Zeolite Catalytic Performance in the Propane-SCR-NOx Process: A Comparative Study. *Int. J. Chem. React. Eng.* **2018**, *16*, 20160192. [CrossRef]
27. Xu, R.; Wang, Z.; Liu, N.; Dai, C.; Zhang, J.; Chen, B. Understanding Zn Functions on Hydrothermal Stability in a One-Pot-Synthesized Cu&Zn-SSZ-13 Catalyst for NH3 Selective Catalytic Reduction. *ACS Catal.* **2020**, *10*, 6197–6212. [CrossRef]
28. Saeidi, M.; Hamidzadeh, M. Co-doping a metal (Cr, Mn, Fe, Co, Ni, Cu, and Zn) on Mn/ZSM-5 catalyst and its effect on the catalytic reduction of nitrogen oxides with ammonia. *Res. Chem. Intermed.* **2017**, *43*, 2143–2157. [CrossRef]
29. Wang, X.; Xu, Y.; Zhao, Z.; Liao, J.; Li, Q. Recent progress of metal-exchanged zeolites for selective catalytic reduction of NOx with NH3 in diesel exhaust. *Fuel* **2021**, *305*, 121482. [CrossRef]
30. Han, L.; Cai, S.; Gao, M.; Hasegawa, J.Y.; Wang, P.; Zhang, J.; Shi, L.; Zhang, D. Selective Catalytic Reduction of NOx with NH_3 by Using Novel Catalysts: State of the Art and Future Prospects. *Chem. Rev.* **2019**, *119*, 10916–10976. [CrossRef]
31. Martín, N.; Paris, C.; Vennestrøm, P.N.R.; Thøgersen, J.R.; Moliner, M.; Corma, A. Cage-based small-pore catalysts for NH_3-SCR prepared by combining bulky organic structure directing agents with modified zeolites as reagents. *Appl. Catal.* **2017**, *217*, 125–136. [CrossRef]
32. Jin, Q.; Fang, D.; Ye, Y.; Hou, S.; He, F.; Xie, J. Cu, Co, or Ni species in exchanged Y zeolite catalysts and their denitration performance for selective catalytic reduction by ammonia. *Appl. Surf. Sci.* **2022**, *600*, 154075. [CrossRef]
33. Brandenberger, S.; Krocher, O.; Tissler, A.; Althoff, R. The State of the Art in Selective Catalytic Reduction of NOx by Ammonia Using Metal-Exchanged Zeolite Catalysts. *Catal. Rev.* **2008**, *50*, 492–531. [CrossRef]
34. Chen, J.; Huang, W.; Bao, S.; Zhang, W.; Liang, T.; Zheng, S.; Yi, L.; Guo, L.; Wu, X. A review on the characterization of metal active sites over Cu-based and Fe-based zeolites for NH_3-SCR. *RSC Adv.* **2022**, *12*, 27746–27765. [CrossRef] [PubMed]
35. Zhong, C.; Wu, C.; Zuo, H.; Gu, Z. Theoretical analyses of NH_3-SCR reaction-mass transferover Cu-ZSM-5. *Can. J. Chem. Eng.* **2022**, *100*, 3081–3436. [CrossRef]
36. Qi, X.; Wang, Y.; Liu, C.; Liu, Q. The Challenges and Comprehensive Evolution of Cu-Based Zeolite Catalysts for SCR Systems in Diesel Vehicles: A Review. *Catal. Surv. Asia* **2022**. [CrossRef]
37. Ren, L.; Zhu, L.; Yang, C.; Chen, Y.; Sun, Q.; Zhang, H.; Li, C.; Nawaz, F.; Meng, X.; Xiao, F.S. Designed copper–amine complex as an efficient template for one-pot synthesis of Cu-SSZ-13 zeolite with excellent activity for selective catalytic reduction of NOx by NH_3. *Chem. Commun.* **2011**, *47*, 9789–9791. [CrossRef]

38. Leistner, K.; Mihai, O.; Wijayanti, K.; Kumar, A.; Kamasamudram, K.; Currier, N.W.; Yezerets, A.; Olsson, L. Comparison of Cu/BEA, Cu/SSZ-13 and Cu/SAPO-34 for ammonia-SCR reactions. *Catal. Today* **2015**, *258*, 49–55. [CrossRef]
39. Kwak, J.H.; Tonkyn, R.G.; Kim, D.H.; Szanyi, J.; Peden, C.H. Excellent activity and selectivity of Cu-SSZ-13 in the selective catalytic reduction of NOx with NH_3. *J. Catal.* **2010**, *275*, 187–190. [CrossRef]
40. Jabłońska, M.; Góra-Marek, K.; Bruzzese, P.C.; Palčić, A.; Pyra, K.; Tarach, K.; Bertmer, M.; Poppitz, D.; Pöppl, A.; Gläser, R. Influence of Framework n(Si)/n(Al) Ratio on the Nature of Cu Species in Cu-ZSM-5 for NH_3-SCR-DeNOx. *ChemCatChem* **2022**, *14*, e202200627. [CrossRef]
41. Gao, F.; Walter, E.D.; Kollar, M.; Wang, Y.; Szanyi, J.; Peden, C.H. Understanding ammonia selective catalytic reduction kinetics over Cu/SSZ-13 from motion of the Cu ions. *J. Catal.* **2014**, *319*, 1–14. [CrossRef]
42. Kurzydym, I.; Czekaj, I. The effect of the presence of a hydroxyl group on the vibration frequencies of NO and NH_3 adsorbates on Cu-Zn bimetallic nanoparticles in ZSM-5 and FAU zeolite—A DFT study. *J. Mol. Struct.* **2022**, *1255*, 132440. [CrossRef]
43. Ho, P.H.; Jabłońska, M.; Nocuń, M.; Fornasari, G.; Ospitali, F.; Vaccari, A.; Benito, P.; Palkovits, R. Effect of Neodymium on the Physico-chemical Properties and N_2O Decomposition Activity of Co(Cu)−Al Mixed Oxides. *ChemCatChem* **2019**, *11*, 5580–5592. [CrossRef]
44. Lykaki, M.; Papista, E.; Carabineiro, S.A.C.; Tavares, P.B.; Konsolakis, M. Optimization of N_2O decomposition activity of CuO–CeO_2 mixed oxides by means of synthesis procedure and alkali (Cs) promotion. *Catal. Sci. Technol.* **2018**, *8*, 2312–2322. [CrossRef]
45. Pietrogiacomi, D.; Campa, M.C.; Carbone, L.R.; Tuti, S.; Occhiuzzi, M. N_2O decomposition on CoO_x, CuO_x, FeO_x or MnO_x supported on ZrO_2: The effect of zirconia doping with sulfates or K^+ on catalytic activity. *Appl. Catal.* **2016**, *187*, 218–227. [CrossRef]
46. Inger, M.; Wilk, M.; Saramok, M.; Grzybek, G.; Grodzka, A.; Stelmachowski, P.; Makowski, W.; Kotarba, A.; Sojka, Z. Cobalt Spinel Catalyst for N_2O Abatement in the Pilot Plant Operation–Long-Term Activity and Stability in Tail Gases. *Ind. Eng. Chem. Res.* **2014**, *53*, 10335–10342. [CrossRef]
47. Gholizadeh, R.; Yu, Y.X.; Wang, Y. N_2O adsorption and decomposition over ZnO(0001) doped graphene: Density functional theory calculations. *Appl. Surf. Sci.* **2017**, *420*, 944–953. [CrossRef]
48. Sun, B.Z.; Chen, W.K.; Wang, X.; Lu, C.H. A density functional theory study on the adsorption and dissociation of N_2O on Cu_2O (111) surface. *Appl. Surf. Sci.* **2007**, *253*, 7501–7505. [CrossRef]
49. Heyden, A.; Peters, B.; Bell, A.T.; Keil, F.J. Comprehensive DFT Study of Nitrous Oxide Decomposition over Fe-ZSM-5. *J. Phys. Chem. B* **2005**, *109*, 1857–1873. [CrossRef]
50. Abu-Zieda, B.M.; Soliman, S.A.; Asiri, A.M. Role of rubidium promotion on the nitrous oxide decomposition activity of nanocrystalline Co_3O_4-CeO_2 catalyst. *Appl. Surf. Sci.* **2019**, *479*, 148–157. [CrossRef]
51. Hu, X.; Wang, Y.; Wu, R.; Zhao, Y. Graphitic carbon nitride-supported cobalt oxides as a potential catalyst for decomposition of N_2O. *Appl. Surf. Sci.* **2021**, *538*, 148157. [CrossRef]
52. Qi, J.; Qi, X.; Pan, Y.; Cui, J.; Xiong, Y.; Shan, W.; Yu, H. Sm doped NiO catalysts with excellent H_2O resistance for N_2O decomposition under simulated nitric acid plant exhaust condition. *Appl. Surf. Sci.* **2023**, *611*, 155657. [CrossRef]
53. Pérez-Ramirez, J.; Kapteijn, F.; Schöffel, K.; Moulijn, J.A. Formation and control of N_2O in nitric acid production. Where do we stand today? *Appl. Catal. B* **2003**, *44*, 117–151. [CrossRef]
54. Pietrzyk, P.; Zasada, F.; Piskorz, W.; Kotarba, A.; Sojka, Z. Computational spectroscopy and DFT investigations into nitrogen and oxygen bond breaking and bond making processes in model deNOx and deN_2O reactions. *Catal. Today* **2007**, *119*, 219–227. [CrossRef]
55. Inger, M.; Rajewski, J.; Ruszak, M.; Wilk, M. The infuence of NO_x presence on the catalytic N_2O decompositionover the supported double-promoted cobalt spinel catalyst. *Chem. Pap.* **2019**, *73*, 1979–1986. [CrossRef]
56. Van den Brink, R.W.; Booneveld, S.; Verhaak, M.J.F.M.; de Bruijn, F.A. Selective catalytic reduction of N_2O and NO_x in a single reactor in the nitric acid industry. *Catal. Today* **2002**, *75*, 227–232. [CrossRef]
57. Wang, Y.; Lei, Z.; Chen, B.; Guo, Q.; Liu, N. Adsorption of NO and N_2O on Fe-BEA and H-BEA zeolites. *Appl. Surf. Sci.* **2010**, *256*, 4042–4047. [CrossRef]
58. Piskorz, W.; Zasada, F.; Stelmachowski, P.; Kotarba, A.; Sojka, Z. DFT Modeling of Reaction Mechanism and Ab Initio Microkinetics of Catalytic N_2O Decomposition over Alkaline Earth Oxides: From Molecular Orbital Picture Account to Simulation of Transient and Stationary Rate Profiles. *J. Phys. Chem. C* **2013**, *117*, 18488–18501. [CrossRef]
59. Chen, B.; Liu, N.; Liu, X.; Zhang, R.; Li, Y.; Li, Y.; Sun, X. Study on the direct decomposition of nitrous oxide over Fe-beta zeolites: From experiment to theory. *Catal. Today* **2011**, *175*, 245–255. [CrossRef]
60. He, G.; Lian, Z.; Yu, Y.; Yang, Y.; Liu, K.; Shi, X.; Yan, Z.; Shan, W.; He, H. Polymeric vanadyl species determine the low-temperature activity of V-based catalysts for the SCR of NOx with NH_3. *Sci. Adv.* **2018**, *4*, eaau4637. [CrossRef]
61. Avdeev, V.I.; Bedilo, A.F. Formation of reactive oxygen by N_2O decomposition over binuclear cationic sites of Fe-ferrierite zeolite: Periodic DFT + U study. *Chem. Phys. Lett.* **2018**, *695*, 222–227. [CrossRef]
62. Gao, C.; Li, J.; Zhang, J.; Sun, X. DFT Study on the Combined Catalytic Removal of N_2O, NO, and NO_2 over Binuclear Cu-ZSM-5. *Catalysts* **2022**, *12*, 438. [CrossRef]
63. Du, X.; Gao, X.; Hu, W.; Yu, J.; Luo, Z.; Cen, K. Catalyst Design Based on DFT Calculations: Metal Oxide Catalysts for Gas Phase NO Reduction. *J. Phys. Chem. C* **2014**, *118*, 13617–13622. [CrossRef]

64. Macrae, C.F.; Sovago, I.; Cottrell, S.J.; Galek, P.T.; McCabe, P.; Pidcock, E.; Platings, M.; Shields, G.P.; Stevens, J.S.; Towler, M.; et al. Mercury 4.0: From visualization to analysis, design and prediction. *J. Appl. Crystallogr.* **2020**, *53*, 226–235. [CrossRef] [PubMed]
65. Portmann, S.; Lüthi, H.P. MOLEKEL: An Interactive Molecular Graphics Tool. *Chimia* **2000**, *54*, 766–769. [CrossRef]
66. Hermann, K.; Pettersson, L.G.M.; Casida, M.E.; Daul, C.; Goursot, A.; Koester, A.; Proynov, E.; St-Amant, A.; Salahub, D.R.; Carravetta, V.; et al. *StoBe-deMon*, deMon Software: Stockholm, Sweden; Berlin, Germany, 2005. Available online: http://www.fhi-berlin.mpg.de/KHsoftware/StoBe/(accessed on 8 August 2023).
67. Perdew, J.P.; Burke, K.; Ernzerhof, M. Generalized Gradient Approximation Made Simple. *Phys. Rev. Lett.* **1996**, *77*, 3865. [CrossRef] [PubMed]
68. Hammer, B.; Hansen, L.B.; Nørskov, J.K. Improved adsorption energetics within density-functional theory using revised Perdew-Burke-Ernzerhof functionals. *Phys. Rev. B* **1999**, *59*, 7413. [CrossRef]
69. Broclawik, E.; Salahub, D.R. Density functional theory and quantum chemistry: Metals and metal oxides. *J. Mol. Catal.* **1993**, *82*, 117. [CrossRef]
70. Mulliken, R.S. Electronic Population Analysis on LCAO–MO Molecular Wave Functions. II. Overlap Populations, Bond Orders, and Covalent Bond Energies. *J. Chem. Phys.* **1955**, *23*, 1833. [CrossRef]
71. Mayer, I. Charge, bond order and valence in the AB initio SCF theory, Chem. *Phys. Lett.* **1983**, *97*, 270. [CrossRef]
72. Mayer, I. Bond orders and valences: Role of d-orbitals for hypervalent Sulphur. *J. Mol. Struct. THEOCHEM* **1987**, *149*, 81–89. [CrossRef]
73. Mills, G.; Jonsson, H. Quantum and thermal effects in H_2 dissociative adsorption: Evaluation of free energy barriers in multidimensional quantum systems. *Phys. Rev. Lett.* **1994**, *72*, 1124. [CrossRef] [PubMed]
74. Mills, G.; Jonsson, H.; Schenter, G.K. Reversible work transition state theory: Application to dissociative adsorption of hydrogen. *Surf. Sci.* **1995**, *324*, 305–337. [CrossRef]
75. Jonsson, H.; Mills, G.; Jacobson, K.W. *Nudged Elastic Band Method for Finding Minimum Energy Paths and Transitions in Classical and Quantum Dynamics in Condensed Phase Simulations*; Berne, B.J., Ciccotti, G., Coker, D.F., Eds.; World Scientific Publishing Company: Singapore, 1998.
76. Henkelman, G.; Uberuaga, B.P.; Jonsson, H. A climbing image nudged elastic band method for finding saddle points and minimum energy paths. *J. Chem. Phys.* **2000**, *113*, 9901–9904. [CrossRef]
77. Koyama, K.; Takéuchi, Y. Clinoptilolite: The distribution of potassium atoms and its role in thermal stability. *Z. Krist.-Cryst. Mater.* **1977**, *145*, 216–239. [CrossRef]
78. Available online: http://www.iza-structure.org/databases/ (accessed on 25 May 2023).
79. Uzunova, E.L.; Mikosch, H. Cation site preference in zeolite clinoptilolite: A density functional study. *Microporous Mesoporous Mater.* **2013**, *177*, 113–119. [CrossRef]